Electronic Supplementary Information

A dual-mode optical biosensor based on multi-functional DNA structures for detecting bioactive small molecules

Li Guo, ‡ Dandan Chen, ‡ Huijie Wang, Xinzhu Meng, Yongcun Yan, Shuangcheng Zhi, Senquan Dai, Sai Bi*

College of Chemistry and Chemical Engineering, Qingdao University, Qingdao, 266071, PR China

‡ These authors contribute equally to this work.

* Corresponding author. E-mail: bisai11@126.com

1. Experimental Section

1.1. Materials and reagents. The oligonucleotides used in this work were synthesized by Sangon Biotech. Co., Ltd. (Shanghai, China), and the sequences were shown in Table S1. T4 DNA ligase, exonuclease I (Exo I), deoxynucleotides (dNTPs), sulfosalicylic acid (SSA), tris(hydroxymethyl) methanamine (Tris), disodium edetate (EDTA) and 2, 2'-azino-bis(3-ethylbenzothiazoline)-6-sulfonate diammonium salt (ABTS) were obtained from Sangon Biotech. Co., Ltd. (Shanghai, China). 2-(N-Morpholino) ethanesulfonic acid (MES) and 4S Red Plus solution were purchased from BBI Life Sciences Co., Ltd. (Shanghai, China). Phi29 DNA polymerase was ordered from HaiGene Biotech Co., Ltd. (Harbin, China). Hemin, ammonium persulfate (APS), poly(L-lysine) (PLL) and dopamine (DA) were ordered from Macklin Biochemical Co., Ltd. (Shanghai, China). N, N, N′, N′-tetramethylethylenediamine (TEMED), sodium acetate and Glutathione (GSH) were obtained from Aladdin Biochemical Technology Co., Ltd. (Shanghai, China). Poly[2-methoxy-5-(2-ethylhexyloxy)-1, 4-(1-cyanovinylene-1, 4-phenylene)] (CN-PPV, average molecular weight: 26000, polydispersity: 2.7) was purchased from American Dye Source (Quebec, Canada). Poly(styrene-co-maleic anhydride) (PSMA, average MW≈ 1700, styrene content 68%) and anhydrous tetrahydrofuran (THF, ≥99.9%) were purchased from Sigma-Aldrich (Shanghai, China). Hydrogen peroxide (H_2O_2, 30 wt%), glacial acetic acid, magnesium chloride ($MgCl_2$), potassium chloride (KCl), sodium dihydrogen phosphate (NaH_2PO_4), disodium hydrogen phosphate (Na_2HPO_4), acrylamide and bovine serum albumin (BSA) were obtained from Sinopharm Chemical Reagent Co., Ltd. (Shanghai, China). The 20-bp DNA ladder (DNA Plus) was bought from Takara (Beijing, China). The 6×loading buffer was obtained from Hunan Accurate Biology Co., Ltd. (Changsha, China). The GSH assay kit was obtained from Solarbio Life Science Co. Ltd. (Beijing, China). All reagents were analytical grade reagents and used without further purification. Ultrapure water (18.2 MΩ·cm) without nuclease was used in the whole experiments.

Table S1. Oligonucleotides used in this work

Strand	Sequence (5'→3')
padlock probe	Phosphate-AGTCGTGTGAGAAAACCCAACCCGCCCTACCCAAAAG ATATCGTCAACATC
primer	TCACACGACT GATGTTGACG

1.2. Apparatus. Scanning electron microscope (SEM) images and X-ray energy spectra were recorded using the Regulus8100 field emission SEM (Hitachi, Japan). The transmission electron microscopy (TEM) images were recorded on a HT7700 field-emission electron microscope operating at 100 kV (HITACHI, Japan). The time-dependent UV-vis absorbance was measured using the Synergy HTX multimode microplate reader (BioTek, USA). The UV-vis absorption spectra were obtained by a UV-2600 spectrophotometer (Shimadzu, Japan). Fluorescence spectra were acquired on a F-7000 Fluorescence spectrophotometer (Hitachi, Japan). The zeta potential measurements were accomplished with a Nano ZSE (Malvern Panalytical). The circular dichroism (CD) measurements were performed on a J-1500 spectropolarimeter (Jasco, Japan). The HPLC measurements were accomplished by Agilent 1260 Infinity II (Agilent, USA).

1.3. Preparation of positively charged Pdots ($Pdots^+$). First, the negatively charged Pdots ($Pdots^-$) were prepared through a reprecipitation method.[1] In brief, the mixture of poly[2-methoxy-5-(2-ethylhexyloxy)-1, 4-(1-cyanovinylene-1, 4-phenylene)] (CN-PPV) and poly (styrene-comaleic anhydride) (PSMA) dissolved in anhydrous tetrahydrofuran (THF) was quickly added to water under sonication. After removing THF on a hot plate (70 °C, 1 h), the solution was concentrated by rotary evaporation and filtered by a 0.22 μm membrane filter. Then, the $Pdots^-$ were modified with poly(L-lysine) (PLL) via an amide coupling reaction. Specifically, the $Pdots^-$ and freshly prepared 1-ethyl-3-(3-(dimethylamino) propyl) carbodiimide (EDC) were mixed in 1× 2-(N-Morpholino) ethanesulfonic acid (MES) buffer (pH 6.5), followed by adding PLL and oscillating for 2 h in the dark. Subsequently, the solution was ultrafiltered with a 100 kDa ultrafiltration tube to remove the excess PLL, producing the $Pdots^+$ aqueous solution, which was stored at room temperature.

1.4. Preparation of PH-DNFs. The circular DNA template was prepared using the primer and the 5′-phosphorylated padlock probe in the presence of T4 DNA ligase. Firstly, 5 μL of padlock probe (100 μM) and 10 μL of primer (100 μM) were mixed in 1× T4 DNA ligase buffer (40 mM Tris-HCl, 10 mM $MgCl_2$, 10 mM DTT, 0.5 mM ATP, pH 7.8). Subsequently, the solution was heated at 95 °C for 5 min and slowly cooled to 25 °C for 3 h to ensure the hybridization of padlock probe with primer. Then, 4 μL of T4 DNA ligase was added to the above annealed mixture and incubated overnight at 16 °C, followed by heating at 65 °C for 10 min to inactivate the ligase. Finally, the product was transferred to 1× Exo I buffer (67 mM glycine-KOH, 6.7 mM $MgCl_2$, 1 mM DTT, pH 9.5) containing 5 μL of Exo I and incubated at 37 °C for 1.5 h

to remove the unreacted primer and padlock, followed by heating at 80 °C for 15 min to inactivate Exo I.

The DNFs were prepared via RCA process. In brief, the reaction was performed in a phi29 polymerase buffer (33 mM Tris-acetate, 10 mM Mg $(CH_3COO)_2$, 66 mM CH_3COOK, 1% Tween 20, 1 mM DTT, pH 7.9) containing the as-prepared circular DNA templates (0.4 μM), dNTPs (1 mM), and phi29 DNA polymerase (0.5 U/μL) at 30 °C for 12 h, followed by incubation at 25 °C for 30 h. Subsequently, the reaction was terminated by heating at 65 °C for 10 min to inactivate phi29 DNA polymerase, and Hemin (2 mM) was added to the mixture followed by incubation for 4 h. Then the reaction solution was centrifuged at 8000 rpm for 10 min and washed with ultrapure water for three times to obtain the purified H-DNFs, which were dispersed in ultrapure water and stored at 4 °C until use. Finally, PH-DNFs were prepared by oscillating the mixture of electronegative H-DNFs and electropositive $Pdots^+$ for 1 h. The product was centrifugated (4000 rpm, 5 min) and washed with ultrapure water for three times to remove the unloaded $Pdots^+$. The obtained DNFs, H-DNFs, and PH-DNFs were dispersed in ultrapure water and stored at 4 °C.

1.5. Preparation of 8% polyacrylamide gel. The 8% polyacrylamide gel was prepared by mixing 2.7 mL of 30% gel solution (acrylamide/bisacrylamide, 29:1), 90 μL of 10% APS, 1 mL of 10× TAE buffer (2 M Tris-acetic acid, 50 mM EDTA, and 250 mM magnesium acetate, pH 8.3), 10 μL of TEMED and 6.2 mL of ultrapure water, which was stood at room temperature for 45 min. Afterwards, 10 μL of each sample was mixed with 2 μL of 6× loading buffer and slowly added into the loading well to perform electrophoresis experiments.

1.6. Quantification of $Pdots^+$ and Hemin in PH-DNFs. The $Pdots^+$ have a maximum emission peak at 590 nm under 457 nm excitation. The loading amount of $Pdots^+$ on PH-DNFs was quantified through the standard curve method. To obtain the standard curve of $Pdots^+$, the $Pdots^+$ solution was diluted to various concentrations (1-10 μg/mL) by water. And the fluorescence intensity was measured at 590 nm using a F-7000 Fluorescence spectrophotometer (Hitachi, Japan). After obtaining the linear relationship between the fluorescence intensity and concentration of $Pdots^+$, the PH-DNFs solution was measured three times in the same way to quantify the loading amount of $Pdots^+$.

The standard curve of Hemin was obtained by mixing 5 μL of Hemin with different concentrations (0.65-6.5 μg/mL) in 1% Na_2CO_3 solution and 95 μL of water at room temperature. The UV-vis absorbance was measured at 400 nm using a Synergy HTX

multi-mode microplate reader (BioTek, USA). After obtaining the linear relationship between the absorption and concentration of Hemin, the PH-DNFs solution was measured three times in the same way to quantify the loading amount of Hemin.

1.7. Catalytic performance of PH-DNFs. The peroxidase-like activity of DNFs, H-DNFs and PH-DNFs was evaluated by monitoring the catalytic oxidation of ABTS in the presence of H_2O_2. The DNFs and PH-DNFs were dispersed in MES buffer (pH 5.5) at a concentration of 5 μg/mL. Then, 6 μL of each solution was mixed with 10 μL of ABTS (20 mM) and 20 μL of H_2O_2 (100 mM), respectively, and further incubated at room temperature for 30 min. Finally, the absorption spectra of the solutions were recorded using a UV-2600 spectrophotometer (Shimadzu, Japan) over a range of 375-500 nm.

The kinetic analysis of the catalytic performance of PH-DNFs was conducted in MES buffer (1×, pH 5.5) containing a certain concentration of ABTS (2 mM) and various concentrations of H_2O_2 (2.5-50 mM), or containing a certain concentration of H_2O_2 (5 mM) and various concentration of ABTS (0.025-0.5 mM). The absorbance of the reaction solutions was recorded at 420 nm in a time scanning mode. To evaluate the affinity of PH-DNFs toward its substrate, the kinetic constants were obtained according to Lineweaver-Burk plots of the Michaelis-Menten equation:[2]

$$\frac{1}{V} = \frac{K_m}{V_{max}} \times \frac{1}{[S]} + \frac{1}{V_{max}}$$

where V is the initial reaction rate, V_{max} is the maximum reaction rate, [S] is the concentration of substrate, and K_m is the Michaelis constant.

1.8. Cell culture. Four human cells lines (human breast cancer cell line MCF-7, human cervical cancer cell line HeLa, the non-small cell lung cancer cell line A549 and the normal human hepatic cell line L-02) were cultured in a Dulbecco's modified Eagle's medium (DMEM) supplemented with 10% fetal bovine serum (FBS) and 1% penicillin-streptomycin (10 000 U/mL) in a humidified 5% CO_2 at 37 °C. When approximately 80% of confluence was reached, the cells were gently rinsed three times with PBS (10 mM, pH 7.4) and digested with trypsin-EDTA solution at 37 °C for 3 min. Finally, the cells were collected by centrifugation (4 °C, 250 g, 5 min) for subsequent experiments.

1.9. Fluorescent/colorimetric dual-mode detection of DA and GSH. For DA detection, 6 μL of PH-DNFs (100 μg/mL) in MES buffer (pH 5.5) were mixed with 2 μL of H_2O_2 (100 mM) and DA solution with varying concentrations. Each mixture was

supplemented with deionized water up to a volume of 40 μL and incubated at room temperature for 30 min. The fluorescence spectra of those samples were measured in the range of 480-700 nm with an excitation wavelength of 457 nm. The fluorescence intensity at 590 nm was used for the quantitative analysis of DA. Subsequently, 10 μL of ABTS (20 mM) and 20 μL of H_2O_2 (100 mM) were added to the mixture and incubated for 1 h. Finally, the UV-vis spectra of the samples were measured in the range of 370-500 nm using a Synergy HTX multimode microplate reader (BioTek, USA).

For GSH detection, 6 μL of PH-DNFs (100 μg/mL) and 20 μL of GSH with varying concentrations were pre-mixed in MES buffer (pH 5.5), followed by adding 4 μL of DA solution (500 μM) and 2 μL of H_2O_2 (100 mM). Each mixture was supplemented with deionized water up to a volume of 40 μL and incubated with at 37 ^oC for 90 min under oscillation. The fluorescence spectra of each sample were recorded according to the method mentioned above. For colorimetric detection of GSH, the samples were centrifuged (4000 rpm, 5 min) and washed with ultrapure water for three times. The obtained precipitates were re-suspended to 40 μL MES buffer, followed by adding 10 μL of ABTS (20 mM) and 20 μL of H_2O_2 (100 mM) and incubating for 60 min. Finally, the absorbance at 420 nm of each sample was measured using a Synergy HTX multi-mode microplate reader.

1.10. Real samples analysis. Serum samples from breast cancer patients were obtained from the Affiliated Hospital of Qingdao University. These samples were treated with acetonitrile in a 2:1 ratio for 5 minutes, followed by centrifugation at 10, 000 rpm for 20 minutes to collect the supernatant. Subsequently, 20 μM of DA in MES buffer (pH 5.5) were spiked into the above obtained serum samples. The procedure of DA detection was performed as mentioned above.

The cell lysis was prepared according to previous reports.[3] In brief, the collected cells (1.5×10^5) were mixed with 80 μL of HCl (10 mM), and subjected to freeze-thawing twice to lyse the cells. Then, 20 μL of 5% 5-sulfosalicylic acid (SSA) was added and centrifuged at 4 ^oC for 10 min (8000 g) to remove the cell debris. Finally, 100 μL of supernatant was collected for GSH detection as mentioned above.

All the experiments involving human samples were conducted in strict accordance with the relevant laws and institutional guidelines, which were approved by the Ethics Committee of Qingdao University Affiliated Hospital.

2. Additional characterization of PH-DNFs

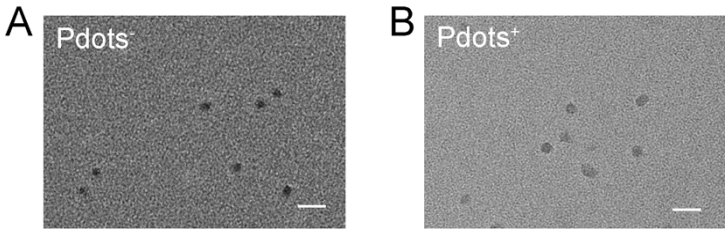

Fig. S1 The TEM images of (A) $Pdots^-$ and (B) $Pdots^+$. Scale bar: 50 nm.

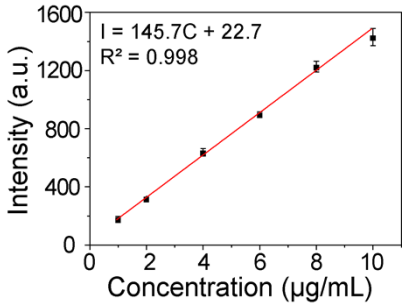

Fig. S2 Calibration curve of fluorescence intensity at 590 nm versus the concentration of $Pdots^+$ solution. Error bars represent the standard deviation of three replicate determinations.

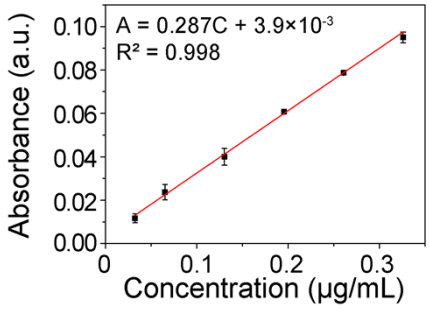

Fig. S3 Calibration curve of UV-vis absorbance at 400 nm versus the concentration of Hemin solution. Error bars represent the standard deviation of three replicate determinations.

The topology of the G-quadruplexes in DNFs and H-DNFs were assessed using circular dichroism (CD). As shown in Fig. S4, the CD spectrum of DNFs exhibits a negative peak near 245 nm and a positive peak near 275 nm. Compared with DNFs, the CD spectrum of H-DNFs shows minimal changes. It indicates the formation of parallel G-quadruplex topologies in both of DNFs and H-DNFs, and G-quadruplexes could maintain their topologies after complexing with Hemin.[4]

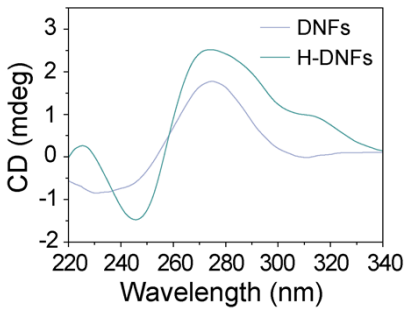

Fig. S4 CD spectroscopy analysis of DNFs and H-DNFs.

To investigate the stability of PH-DNFs at different pH, the morphological change of PH-DNFs were tracked using SEM, with H-DNFs used as control. As shown in Fig. S5, both H-DNFs and PH-DNFs are stable at 2-(N-Morpholino) ethanesulfonic acid (MES) buffer (pH 8.0). However, after incubating in MES buffer (pH 5.0) for 30 min, H-DNFs display obvious morphological changes, including a blurred sheet structure and a collapsed flower-like structure. On the contrary, the PH-DNFs maintain the structural integrity even after incubating at pH 5.0 for 90 min, indicating that $Pdots^{+}$ may play an important role in improving the stability of DNFs.

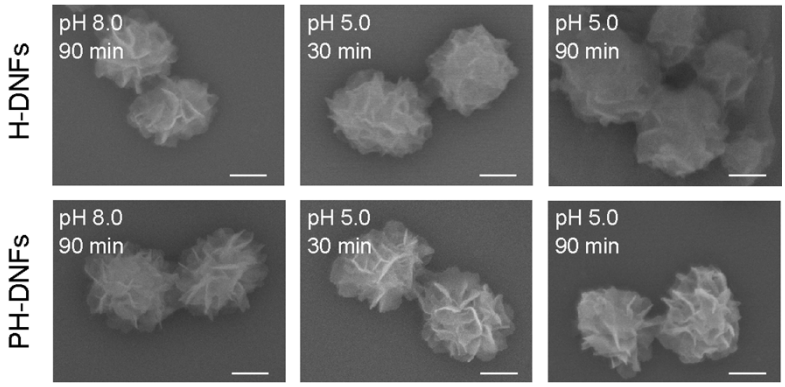

Fig. S5 SEM images of H-DNFs and PH-DNFs after incubation at different pHs for different times. Scale bar: 250 nm.

3. Peroxidase-like activity of PH-DNFs

For RCA reaction, the template with its two ends capable of hybridizing with the primer is specifically designed to include a sequence complementary to G-quadruplex (G4) sequence. After an annealing process, the template is hybridized with the primer and subsequently circularized by T4 DNA ligase. With the assistance of phi29 DNA polymerase and dNTPs, the circular DNA template is amplified by RCA reaction to obtain long ssDNA with numerous G4 sequences. These sequences fold into G-quadruplex structures in the presence of potassium ions (K^{+}) and then self-assembled

to form flower-like DNA nanostructure containing abundant G-quadruplex structure.[5] In the presence of hemin, the G-quadruplex structure bind with hemin via π-π stacking interactions,[6] resulting in the formation of hemin-encapsulated DNFs (H-DNFs). The H-DNFs were further incubated with positively charged $Pdots^+$ to construct the PH-DNFs.

We assessed the peroxidase-like activity of PH-DNFs by monitoring the catalytic oxidization of ABTS by H_2O_2 to produce chromogenic products $ABTS^{\bullet+}$ (Fig. S6A). As shown in Fig. S6B, upon adding PH-DNFs to the ABTS-H_2O_2 system, obvious absorption peak of $ABTS^{\bullet+}$ at 420 nm is observed, while a negligible absorption is observed for DNFs. These results verify PH-DNFs, which contain G4/Hemin structure, possess peroxidase-like activity.

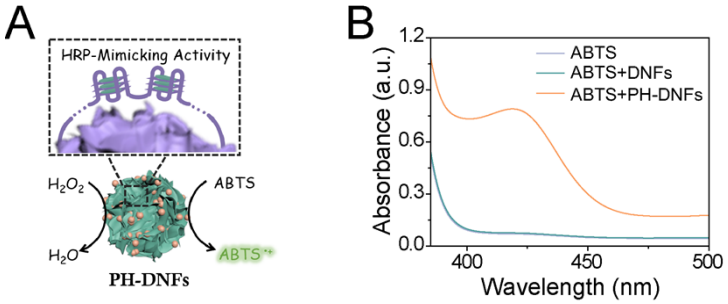

Fig. S6 (A) Schematics of ABTS oxidation by H_2O_2 catalyzed by PH-DNFs. (B) UV-vis absorption spectra of ABTS, ABTS + DNFs, and ABTS + PH-DNFs in the presence of H_2O_2.

Furthermore, we evaluated the effect of pH and buffer solution on the catalytic activity of PH-DNFs. As shown in Fig. S7A, the absorption at 420 nm increases with the decrease in pH from 8.0 to 5.5, verifying the peroxidase-like activity of PH-DNFs is significantly enhanced at lower pH, which is consistent with previous reports.[7] In addition, PH-DNFs in non-ionic MES buffer exhibit higher peroxidase-like activity than that in ionic buffer (Fig. S7B). This can be attributed to the fact that high ionic strength and cation concentration in the ionic buffer may shield the negative charges of the DNA backbone.[7] As K^+ can stabilize G-quadruplex structure and improve the peroxidase-like activity, we optimized the concentration of K^+ in the reaction solution. As shown in Fig. S7C, the peroxidase-like activity of PH-DNFs was obviously enhanced with an increase in the concentration of K^+.[7] Overall, to ensure the highly catalytic activity of PH-DNFs, the reaction was performed in MES buffer (pH 5.5) supplemented with 10 mM K^+.

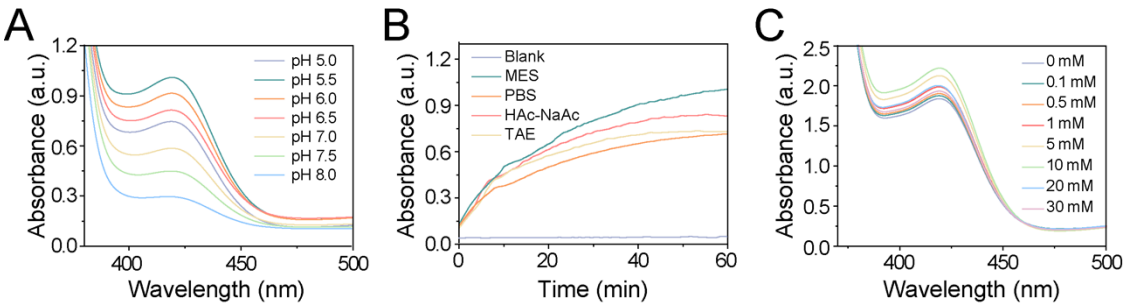

Fig. S7 (A) UV-vis absorption spectra of ABTS-H_2O_2 catalyzed by PH-DNFs at different pHs. (B) Time-dependent absorbance (at 420 nm) of ABTS-H_2O_2 catalyzed by PH-DNFs in different buffers (Blank: ABTS aqueous solution without adding PH-DNFs and H_2O_2). (C) UV-vis absorption spectra of ABTS-H_2O_2 catalyzed by PH-DNFs in MES buffers containing different concentrations of K^+.

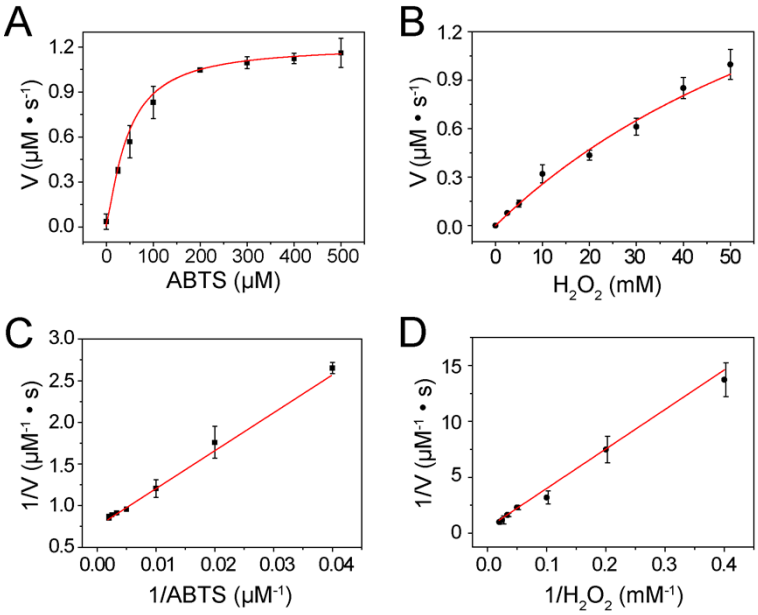

Fig. S8 Kinetic curves of PH-DNFs fitted by Michaelis-Menten equation under different concentrations of (A) ABTS and (B) H_2O_2. Lineweaver–Burk plots of ABTS-H_2O_2 catalyzed by PH-DNFs for (C) ABTS, and (D) H_2O_2. Error bars represent the standard deviation of three replicate determinations.

Table S2. The kinetic parameters of PH-DNFs

	Substrates	V_{max} ($\times 10^{-6}$ M · s^{-1})	K_m (mM)
PH-DNFs	ABTS	1.352	0.0616
	H_2O_2	3.27	0.116

4. Feasibility of this assay

Owing to PH-DNFs with excellent fluorescent property and peroxidase-like activity, a dual-mode detection system based on PH-DNFs was designed for the detection of DA and GSH, respectively. Firstly, the spectral characterization was performed to investigate the feasibility of the assay. As shown in Fig. S9A, in situ polymerization of DA catalyzed by PH-DNFs was monitored by UV-vis absorbance spectroscopy. As expected, the absorption in the range of 550-850 nm increases with increasing reaction time. However, a control reaction conducted using DNFs (without G4/Hemin structure) as a catalysis do not show obvious change in absorbance (Fig. S10). These results demonstrate that the peroxidase-like activity of PH-DNFs is essential for the production of PDA. The produced PDA is likely assembled on the surface of PH-DNFs via π-π interaction. Moreover, the PH-DNFs show a characteristic emission peak at 590 nm under 457 nm excitation (Fig. S9B). In the presence of DA, the fluorescence intensity of PH-DNFs is remarkably reduced. It is because PDA has a broad absorbance from UV-vis to near-infrared, which overlaps well with the emission of $Pdots^{+}$ and enables the resonance energy transfer from $Pdots^{+}$ to PDA, leading to reduced fluorescence signal. Further, the absorption spectra of PH-DNFs-catalyzed ABTS oxidation by H_2O_2 in the absence and presence of DA were monitored. In the absence of DA, a characteristic absorption peak of oxidized ABTS is observed at 420 nm (Fig. S9C), while a decrease in absorbance was observed in the presence of DA. It may be explained as the G4/Hemin structure on PH-DNFs was shield by PDA, resulting in reduced peroxidase-like activity of PH-DNFs. However, upon addition of GSH into the DA reaction solution, both of the fluorescence intensity and absorption increase (Fig. S9B and Fig. S9C). This phenomenon can be explained as the reductive GSH competes with DA for the substrate H_2O_2 and reacts with quinone-rich PDA via a Michael addition reaction, thereby recovering peroxidase-like activity and fluorescent signal of PH-DNFs.[8,9] The above results demonstrate the feasibility of the PH-DNFs-based sensing system for fluorometric/colorimetric dual-mode detection of DA and GSH.

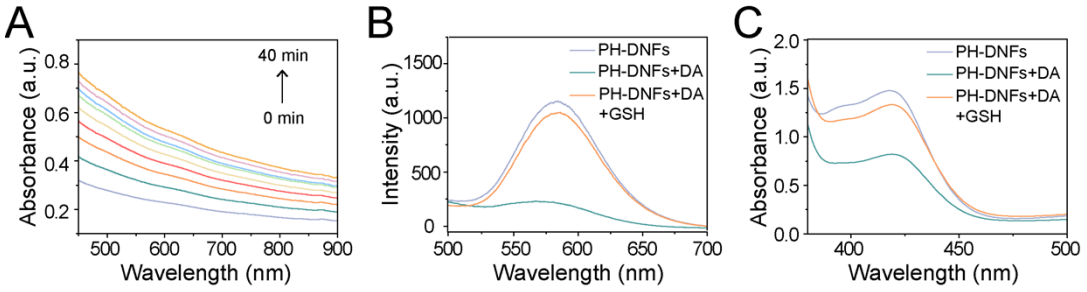

Fig. S9 (A) Time-dependent absorption of H_2O_2-oxidized DA in the presence of PH-DNFs. (B) fluorescence spectra and (C) UV-vis absorption spectra of samples: ABTS + PH-DNFs, ABTS + PH-DNFs + DA, and ABTS + PH-DNFs + DA + GSH.

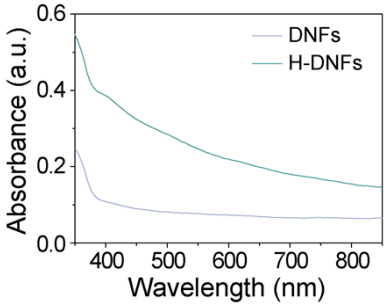

Fig. S10 UV-vis spectra of DA polymerization catalyzed by DNFs (without G4/Hemin structure) and H-DNFs after 30 min, respectively.

5. Dual-mode sensing of GSH in "signal-on" type

Since the reducibility of GSH provides the possibility for competing reaction, the DA polymerization on the surface of PH-DNFs can be blocked by GSH. Therefore, the proposed biosensor based on PH-DNFs was further used for GSH detection in a signal-on type (Fig. 11A). For fluorescent channel, an enhanced fluorescence intensity at 590 nm is observed as the concentration of GSH increases (Fig. 11B). A good linear relationship is obtained between fluorescence intensity and GSH concentration ranging from 0.01 to 1 mM (Fig. 11C). The LOD is calculated to be 9.08 μM. For colorimetric detection, the absorbance of $ABTS^{\bullet+}$ at 420 nm gradually increases as increasing the concentration of GSH (Fig. 11D). The linear correlation is obtained between the absorption value and GSH concentration in the range of 10 to 500 μM with a LOD of 8.77 μM (Fig. 11E). Compared with the reported biosensors for GSH detection (Table S4), the constructed dual-mode biosensors exhibit a high precision and reliability. Moreover, the specificity for GSH was studied by measuring a series of common interfering substances using colorimetric mode and fluorescent mode, respectively. As shown in Fig. 11F and Fig. 11G, no obvious increases of fluorescence emission at 590 nm and absorption at 420 nm are observed for the interfering substances, while a dramatic increase in fluorescence and absorbance is detected for GSH, demonstrating good specificity of the constructed biosensor for GSH detection. Overall, the above results indicate the great potential of the constructed biosensor in GSH detection for disease diagnosis.

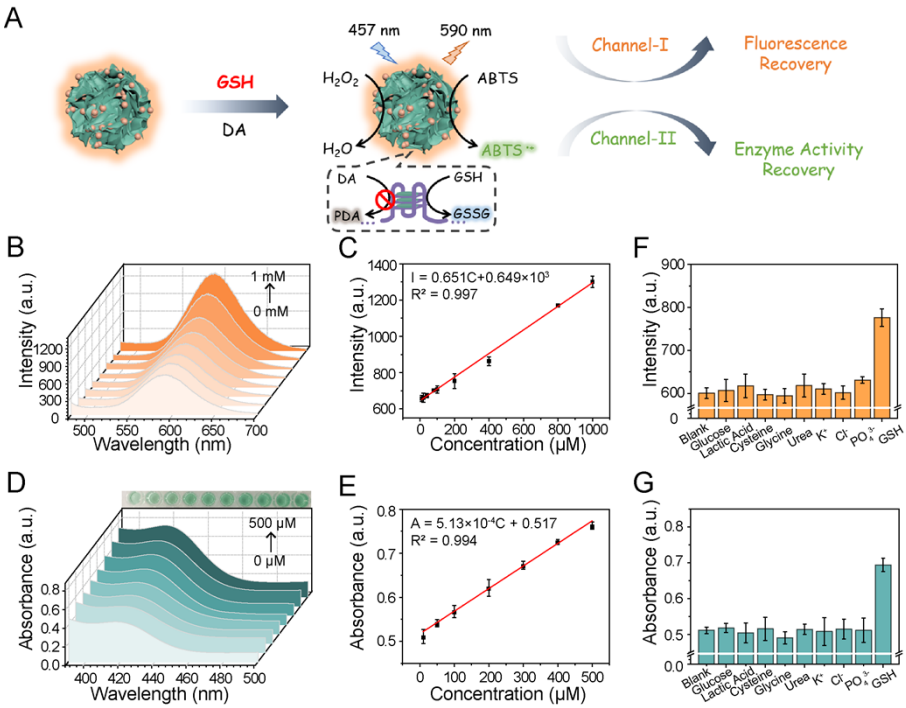

Fig. S11 (A) Schematics of "signal-on" fluorescent/colorimetric dual-mode sensing of GSH. (B) Fluorescence spectra of the proposed biosensor in response to different concentrations of GSH. (C) Linear relationship between fluorescent intensity at 590 nm and the concentration of GSH concentration. (D) UV-vis absorption spectra of the proposed biosensor in response to different concentrations of GSH. (E) Linear relationship between the absorbance of $ABTS^{\bullet+}$ at 420 nm and the concentration of GSH. Specificity of the dual-mode biosensor towards GSH (0.3 mM) compared to a series of interfering substances (1.5 mM) using (F) fluorescent mode and (G) colorimetric mode, respectively. The error bars represent standard deviations from three replicate determinations.

Table S3. Comparison of the proposed dual-mode sensing strategy with other methods for DA detection

Materials	Methods	LOD	Linear Range (μM)	Ref.
CD	Fluorescence	5.54 μM	3.3-500	10
NCD	Fluorescence	5.12 μM	3.3-400	10
CdTe@H-ZIF-8/CDs@MIPs	Fluorescence	12.35 nM	0-0.6	11
PNPG-PEG	Colorimetry	4.6 μM	5.1-125	12
2D VO_2 NS	Colorimetry	5.54 μM	10-500	13
	Fluorescence	3.98 μM	10-375	
AuNPs	Colorimetry	1.23 μM	5-64	14
Zr-NDI/MWCNT	Fluorescence	2 μM	10-100	15
PH-DNFs	Colorimetry	0.996 μM	1-2000	This work
	Fluorescence	0.69 nM	0.1-10000	

Table S4. Comparison of the proposed dual-mode sensing strategy with other methods for GSH detection

Materials	Methods	LOD	Linear Range (μM)	Ref.
Fe-N-C SANs	Colorimetry	78.33 μM	100-400	[16]
Fe NPs	Colorimetry	8.8 μM	10-1000	[17]
Cdots@L-Mn NS	Fluorescence	15 μM	50-200	[18]
B-GQDs-Mn^{7+}	Fluorescence	27 μM	100-500	[19]
Cy-AuNCs	Colorimetry	10 μM	10-400	[20]
PH-DNFs	Colorimetry	8.77 μM	10-500	This work
	Fluorescence	9.08 μM	10-1000	

Table S5. Determination of DA in serum samples using the proposed dual-mode biosensor and HPLC

Methods	No.	DA added (μM)	Found (μM) [a]	Recovery (%)	RSD (%)
Fluorescence	1	20.00	21.81	109.03	5.03
	2	20.00	22.27	111.34	4.93
Colorimetry	1	20.00	21.29	106.45	4.83
	2	20.00	19.93	99.63	5.00
HPLC	1	20.00	21.37	106.87	0.71
	2	20.00	20.09	100.44	1.82

[a]The results are obtained from three duplicate determinations.

References

1. D. Chen, Y. Liu, Z. Zhang, Z. Liu, X. Fang, S. He and C. Wu, *Nano Lett.*, 2021, **21**, 798-805.

2. B. Jiang, D. Duan, L. Gao, M. Zhou, K. Fan, Y. Tang, J. Xi, Y. Bi, Z. Tong, G. F. Gao, N. Xie, A. Tang, G. Nie, M. Liang and X. Yan, *Nat. Protoc.*, 2018, **13**, 1506.

3. X. Wang, Y. Yan, S. Zhi and S. Bi, *Sens. Actuators B Chem.*, 2022, **373**, 132745.

4. Y. Wang, J. Xiao, X. Lin, A. Waheed, A. Ravikumar, Z. Zhang, Y. Zou and C. Chen, *Biosensors*, 2023, **13**, 761.

5. J. Lv, Y. Dong, Z. Gu and D. Yang, *Chem. Eur. J.*, 2020, **26**, 14512.

6. Y. Shi, W. T. Huang, H. Q. Luo and N. B. Li, *Chem. Commun.*, 2011, **47**, 4676.

7. Y. Tokura, S. Harvey, C. Chen, Y. Wu, D. Y. W. Ng and T. Weil, *Angew. Chem. Int. Ed.*, 2018, **57**, 1587.

8. Y. N. Hao, A. Q. Zheng, T. T. Guo, Y. Shu, J. H. Wang, O. Johnson and W. Chen, *J. Mater. Chem. B*, 2019, **7**, 6742.

9. T. H. Wang, M. Y. Shen, N. T. Yeh, Y. H. Chen, T. C. Hsu, H. Y. Chin, Y. T. Wu, B. S. Tzang and W. H. Chiang, *J. Colloid Interface Sci.*, 2023, **650**, 1698.

10. A. Tiwari, S. Walia, S. Sharma, S. Chauhan, M. Kumar, T. Gadly and J. K. Randhawa, *J. Mater. Chem. B*, 2023, **11**, 1029.

11. X. Liu, Y. Fang, D. Zhu, J. Wang, Y. Wu, T. Wang and Y. Wang, *Analyst*, 2023, **148**, 2844.

12. M. Razavi, A. Barras, S. Szunerits, M. Khoshkam, M. Kompany-Zareh and R. Boukherroub, *Anal. Chim. Acta*, 2022, **1235**, 340493.

13. H. Weerasinghe, M. Kumarihamy and H.-F. Wu, *ACS Appl. Mater. Interfaces*, 2023, **15**, 47921.

14. C. Guo, D. Liu, W. Xu, L. He and S. Liu, Colloids Surf. *Colloids Surf. A Physicochem. Eng. Aspects*, 2023, **658**, 130555.

15. G. Radha, K. S. Kumar, K. N. Chappanda and H. Aggarwal, *J. Phys. Chem. C.*, 2023, **127**, 8864.

16. W. Lu, S. Chen, H. Zhang, J. Qiu and X. Liu, *J. Materiomics*, 2022, **8**, 1251.

17. L. Zhang, J. Wang, C. Zhao, F. Zhou, C. Yao and C. Song, *Sens. Actuators B Chem.*, 2022, **361**, 131750.

18. N. Sohal, B. Maity and S. Basu, *ACS Appl. Nano Mater.*, 2020, **3**, 5955.

19. A. Kundu, B. Maity and S. Basu, *New J. Chem.*, 2022, **46**, 7545.

20. C. Jiang, C. Zhang, J. Song, X. Ji and W. Wang, *Spectrochim. Acta. A Mol. Biomol. Spectrosc.*, 2021, **250**, 119316.